

## Thermal Effects on the Stability of Piezoelectric Transformers Based Ballasts for Cold Cathode Fluorescent Lamps

Mor Mordechai Peretz and Sam Ben-Yaakov

Power Electronics Laboratory  
Department of Electrical and Computer Engineering  
Ben-Gurion University of the Negev  
P.O.Box 653, Beer-Sheva 84105, ISRAEL  
Tel: +972-8-6461561; Fax: +972-8-6472949  
Email: sby@ee.bgu.ac.il ; Website: http://www.ee.bgu.ac.il/~pel

**Abstract**— The Envelope Impedance (EI) concept was used to investigate the thermal effects on the stability of Piezoelectric Transformers (PT) based ballasts for Cold Cathode Fluorescent Lamps (CCFL) systems. The envelope analysis of the CCFL, which was verified experimentally, revealed that the magnitude of the negative EI decreases with temperature. This might cause the system to become unstable at low temperatures due to the fact that the loop gain of the PT-CCFL system might encircle the (-1, 0) point in the Nyquist plan. In such cases, the PT-CCFL system may enter a quasi-stable oscillatory operation mode in which the current is AM modulated by a low frequency parasitic signal. This phenomenon is analyzed and explained by considering the temperature effect on the EI of the CCFL. The results of this work provide an insight into the stability issue of the PT-CCFL system, and could help in finding remedies to the instability.

### I. INTRODUCTION

Piezoelectric transformer (PT) based electronic ballasts for Cold Cathode Fluorescent Lamps (CCFL), such as the half-bridge (HB) inverter configuration of Fig. 1, were previously shown to be prone to instabilities [1-3]. Unstable operation may result in light flickering and extra voltage and current stresses, and in severe cases, may cause a runaway situation that will damage the lamp and the PT.

The stability condition of such PT-CCFL systems was examined in earlier studies by small-signal analysis and envelope simulation based on phasor transformation [1-4]. Still lacking, however, is an understanding of a number of phenomena related to this instability. For example, the reason that the system may be unstable at turn-on and then becomes stable after some warm up period. Another issue that needs clarification is the mechanism by which a PT-CCFL system, operating in open loop and driven by a constant frequency, will enter a stable oscillation condition with a constant modulation depth, as seen in Fig. 2. A possible explanation to these effects is a temperature dependence of the lamp's V-I curve that may cause a drift in the stability conditions on the PT-CCFL system.

In this study, we applied the envelope analysis and simulation concept to explore thermal effects on the operating conditions and the oscillation mechanism in PT based CCFL ballast systems.

### II. STABILITY CRITERION

Following [2, 5], we can consider the PT-CCFL system operating in open loop (Fig. 3) as a feedback system (Fig. 4). It should be noticed that the relevant impedances of both elements are their Envelope Impedances (EI) [2, 5]. The EI is defined here as the ratio of the envelope of the voltage, to the envelope of the current, when the impedance is driven by an AM modulated signal. The stability of the PT-CCFL system can thus be studied by analyzing the loop gain (LG) of the feedback loop of Fig. 4 [2, 5]:

$$LG(T) = \frac{Z_{ECCFL}(T)}{Z_{EPT}} \quad (1)$$

where  $Z_{EPT}$  is the EI of the PT and  $Z_{ECCFL}$  is the EI of the lamp which is already assumed here to be a function of temperature  $T$ .

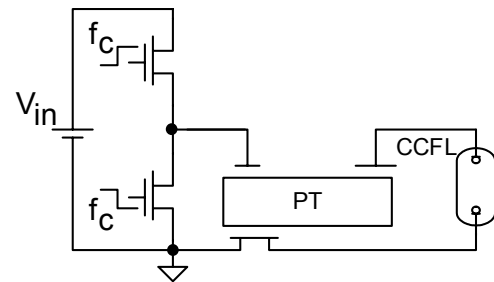


Figure 1. PT-CCFL ballast system driven by half-bridge power stage.

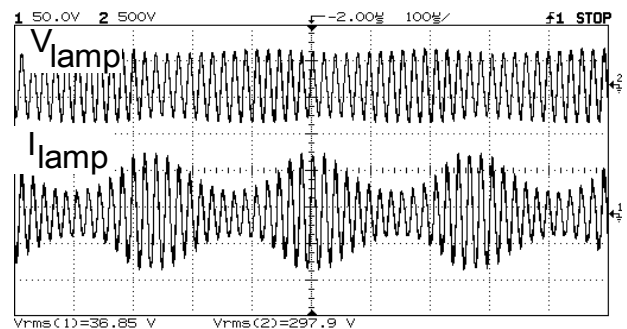


Figure 2. Measured CCFL voltage (0.5KV/div) and current (3.3mA/div) when driven by a PT based HF electronic ballast. Horizontal scale 0.1ms/div.

Equation (1) implies that instability is reached when the EI ratio will encircle the  $(-1, 0)$  point in the Nyquist plan. This will occur if:

$$\left| \frac{Z_{E_{CCFL}}(T)}{Z_{E_{PT}}} \right| \geq 1 \quad (2)$$

when the phase of LG,  $\varphi(LG)$ , is  $(-180^\circ)$ .

### III. ENVELOPE IMPEDANCES (EI)

#### a. Output EI of a PT

The one-mode equivalent circuit of a PT (Fig. 5) can be used to obtain its EI as a function of the modulating frequency  $Z_{E_{PT}}(f_m)$  for a given carrier frequency,  $f_c$ . This was done, in present study, by envelope simulation [6-9]. A typical EI plot of the experimental PT is shown in Fig. 6.

#### b. EI of a CCFL

Earlier studies have shown [5, 10, 11] that the EI of a CCFL driven by a high frequency carrier  $f_c$ ,  $Z_{E_{CCFL}}$ , can be expressed as a function of the modulating frequency  $f_m$  as:

$$Z_{E_{CCFL}}(T) = R_s(T) \frac{\frac{jf_m}{f_p} \cdot \frac{R_{eq}(T)}{R_s(T)} - 1}{\frac{jf_m}{f_p} + 1} \quad (3)$$

where  $R_{eq}(T)$  is the AC resistance of the lamp at the given operating point under a high frequency,  $f_c$ , excitation and  $R_s(T)$  is a constant of the lamp obtained from a static set of V-I measurements of the CCFL [10] - all assumed to be temperature dependent. The relaxation time of the lamp's plasma ( $1/2\pi \cdot f_p$ ) was found, in present study, to be practically independent of the temperature for the present experimental temperature range (will be discussed in the experimental section below).

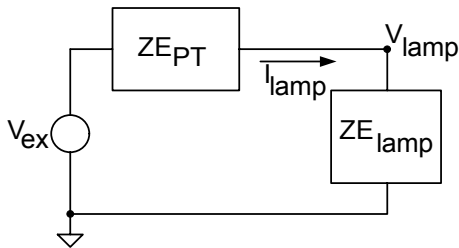


Figure 3. Simplified PT-CCFL ballast system.

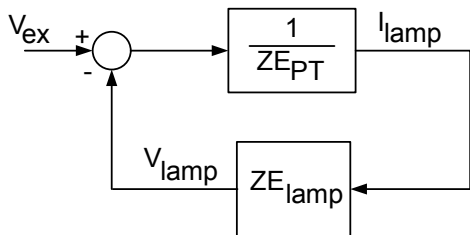


Figure 4. PT-CCFL ballast system represented as a feedback loop.

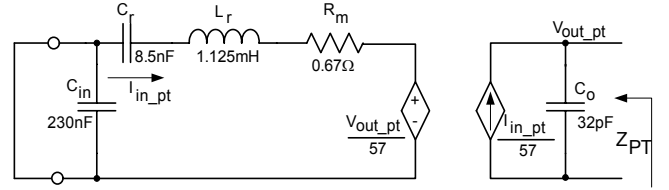


Figure 5. PT equivalent circuit and parameters, connected in the output impedance measurement setup.

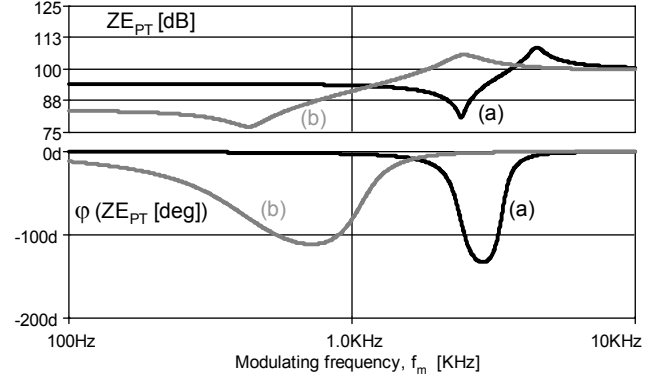


Figure 6. Envelope Impedance of experimental PT (ELECERAM ELM-610) for two carrier frequencies: (a) Operation far from output impedance resonance of the PT  $f_c=49$  KHz and (b) Operation near resonance  $f_c=51$  KHz. ( $f_r=51.5$  KHz)

A convenient way to obtain  $Z_{E_{CCFL}}$  is by running a simulation on a behavioral model of the CCFL [5, 10]. A typical EI plot (of the experimental CCFL), which supports the results of Eq. 3, is depicted in Fig. 7. It shows that at low modulating frequencies ( $f_m < f_p$ )  $Z_{E_{CCFL}}$  is negative, approaching  $(-R_s)$  at  $(f_m \rightarrow 0)$  while at high frequencies ( $f_m \rightarrow \infty$ ) the EI becomes positive.

### IV. STABILITY OF PT-CCFL SYSTEM

Expression (3) shows that at low modulating frequencies ( $f_m < f_p$ )  $Z_{E_{CCFL}}$  is negative, approaching  $(-R_s)$ . Hence, the ratio of  $Z_{E_{CCFL}}$  to  $Z_{E_{PT}}$  (Eq. 1) may indeed reach, at low frequencies, a phase shift of  $-180^\circ$ . The ratio will be larger than  $-1$  (Eq. 1) if:

$$|Z_{E_{CCFL}}(T)| > |Z_{E_{PT}}| \quad (4)$$

That is, the system will be unstable when the absolute value of the negative EI of the CCFL is larger than the positive EI of the PT. As pointed out earlier [2],  $Z_{E_{PT}}$  is expected to have a minimum for  $f_m \approx |f_c - f_r|$ . Hence, the system will be unstable if the EI of the CCFL exhibits a large negative resistance value.

### V. EXPERIMENTAL

The experimental system included a HB inverter feeding a multilayer PT (ELECERAM ELM-610) that was driving a CCFL (JKL BF3250-20B, 3.2mm diameter, 250mm long, 5mA rms nominal current and 520V rms nominal voltage).

The PT's model parameters were obtained by first measuring the PT input to output transfer ratio (TR) and

then applying the PSpice optimization tool [12] to extract the parameters. This add-on package allows the selection of components values to meet a specific goal function. The initial data that are fed to the optimizer include an expression of the goal function, additional constrains, if any, and initial values of the components to be optimized.

The optimization routine was set to search for the values of the model template of Fig. 5, such that it will minimize the squared error between the measured and simulated TRs [2]. The estimated values are given in Fig. 5.

The static V-I curves of the experimental lamp was measured for two thermal operating points (forced air flow, FAF, and natural convection, NC) and are given in Fig. 8. The FAF experiments were carried out by cooling the lamp with two 220V/17W fans. The lamp surface temperature was measured by thermaCAM E45 (FLIR systems) infrared thermal camera. The temperature measurements were taken at a fixed lamp current of 3mA for two the thermal states (FAF and NC). The recorded data were then used to extract the parameters of the SPICE-compatible lamp model (Fig. 9) [5, 10].

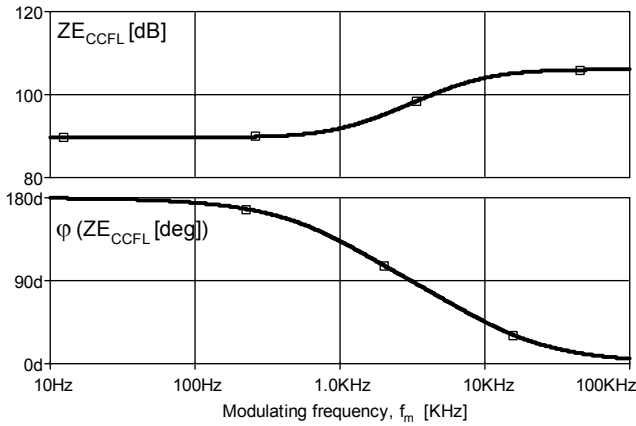


Figure 7. Envelope Impedance of experimental CCFL (JKL BF3250-20B).

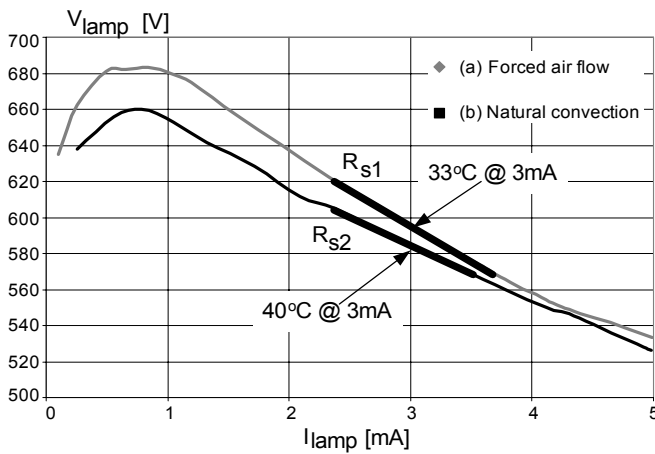


Figure 8. Measured static V-I curves of experimental CCFL (JKL BF3250-20B) operating in two thermal operating conditions: (a) Forced air flow. (b) Natural convection.

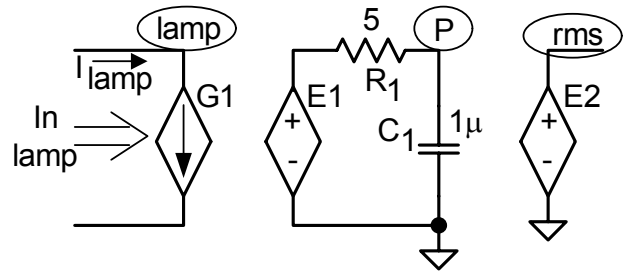


Figure 9. CCFL behavioral model.

In this model the lamp is represented by a dependent current source ( $G_1$ , Fig. 9) that emulates a variable resistance:

$$G_1(\text{FAF}) = \frac{V(\text{lamp})}{\frac{723}{V(\text{rms})} + 1.13 \cdot 10^6 \cdot V(\text{rms}) - 45 \cdot 10^3} \quad (5)$$

$$G_1(\text{NC}) = \frac{V(\text{lamp})}{\frac{690}{V(\text{rms})} + 1.13 \cdot 10^6 \cdot V(\text{rms}) - 38.6 \cdot 10^3} \quad (6)$$

where  $V(\text{lamp})$  is the lamp rms voltage, and  $V(\text{rms})$  is a voltage that emulates the rms lamp current. The denominators of (5) and (6) represent the CCFL equivalent resistance curve under a given thermal operating conditions (forced air flow and natural convection respectively). The constants of equations (5, 6) were estimated by fitting the measured V-I data of Fig. 8 to the template of (5) and (6) for each thermal condition case [10].

The lamp's model includes a dependent voltage source  $E_1$  (Fig. 9) that is defined as the square of the lamp current  $\{(I_{\text{lamp}})^2\}$ .

$$E_1 = (I_{\text{lamp}})^2 \quad (7)$$

The output voltage of  $E_1$  is then passed thru a low-pass network ( $R_1, C_1$ , Fig. 9) to extract the low frequency component [5]. The average voltage of  $C_1$  (node 'P' in Fig. 9) is thus a smoothed value of the square rms current. The filtered rms current is then calculated by  $E_2$  (node 'rms' in Fig. 9) as the square root of  $V(P)$ .

$$E_2 = \sqrt{V(P)} \quad (8)$$

The value of the time constant  $R_1 C_1$  was estimated by matching the envelope response of the model to experimental results. This was done, in present study, by subjecting the PT-CCFL system to a HF carrier that is FM modulated. This caused the lamp current and voltage to be AM modulated due to the reactive nature of the PT (Fig. 5) [13, 14]. The time constant  $R_1 C_1$  (Fig. 9) was then adjusted to match the model simulated results to the measured response over a modulating frequency of 100Hz to 4kHz.

Fig. 10 shows the measured and simulated EI of the experimental CCFL for the two thermal operating conditions (both for a lamp current of 3mA). Simulation

was carried out by the CCFL SPICE model of Fig. 9 after the adjustment of the time constant  $R_1C_1$ . The plots show that  $|Z_{E_{CCFL}}|$  decreases as the temperature  $T$  increases. However, the phase  $\phi(Z_{E_{CCFL}})$  approximately maintains the same frequency response. This implies that the relaxation time of the lamp's plasma can be considered, as first approximation, independent of the temperature for the experimental conditions. The results of the simulated EI of Fig. 10 were obtained with a fixed time constant. The value of the time constant was estimated from the set of measurements at 33°C. The 40°C simulation was carried out with same time constant while applying the relevant current source G1 (Fig. 9) of (6).

## VI. EXTENDED LAMP MODEL

The lamp model of Fig. 9, in conjunction with (5) or (6) is correct for one thermal cooling condition. Assuming that for a small temperature range, the constants of G1 (equations (5), (6)) are, to a first approximation, linear with temperature, the CCFL model can be extended to cover a range of thermal operation conditions. This can be accomplished by the following steps:

### a. Measuring the V-I curves of the lamp under two thermal operating conditions.

Denoting the lamp surface temperatures as  $T_{OH}$  for the high temperature case (lower cooling condition) and  $T_{OL}$  for the low temperature case corresponding the higher cooling condition (each measured for the same reference lamp current) the temperature span would be:

$$\Delta T = T_{OH} - T_{OL} \quad (7)$$

The lamp current sources (G1, Fig. 9) for the two cases can be expressed as:

$$G1_L = \frac{V(\text{lamp})}{\frac{K1_L}{V(\text{rms})} + K2_L \cdot V(\text{rms}) + K3_L} \quad (8)$$

$$G1_H = \frac{V(\text{lamp})}{\frac{K1_H}{V(\text{rms})} + K2_H \cdot V(\text{rms}) + K3_H} \quad (9)$$

where  $K1 - K3$  are the fitted coefficients of the lamp resistance [5], and the subscripts 'L' and 'H' designate the low and high temperature cases, respectively.

### b. Combining (8) and (9) into a single expression by including the temperature dependence.

$$G1_T = \frac{V(\text{lamp})}{\frac{K1_T}{V(\text{rms})} + K2_T \cdot V(\text{rms}) + K3_T} \quad (10)$$

where,

$$K1_T = K1_L - \frac{(T - T_{OL})(K1_L - K1_H)}{\Delta T}$$

$$K2_T = K2_L - \frac{(T - T_{OL})(K2_L - K2_H)}{\Delta T}$$

$$K3_T = K3_L - \frac{(T - T_{OL})(K3_L - K3_H)}{\Delta T},$$

$T$  is the lamp surface temperature for a given cooling condition and the reference lamp current.

A further extension to the model, which was not done in present study, can be accomplished by extracting, experimentally, the relationship between the lamp surface temperature and the cooling air flow of the lamp.

$$T = f(\text{air flow}) \quad (11)$$

Once this relationship is obtained, it can be used to make (10) a function of the air-flow

Fig. 11 shows the measured V-I curves of the CCFL compared to the simulated results of the lamp model using (10). Also depicted in Fig. 11 is the static incremental resistance,  $R_s$  (local slope of the fitted V-I curve) which is found to decrease with an increase in  $T$ . This implies that at cooler ambient temperature the PT-CCFL system is prone to instabilities since the lamp's incremental resistance is increased and hence the ratio of (4) is likely to be satisfied.

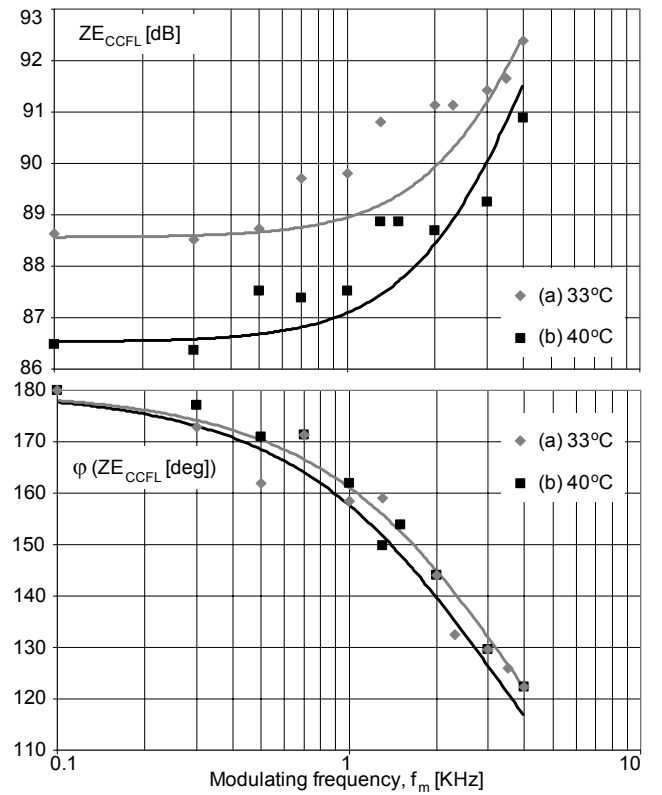


Figure 10. Measured (symbols) and simulated (solid lines) magnitude and phase EI of experimental CCFL (JKL BF3250-20B) in two thermal bias points: (a) 33°C. (b) 40°C.

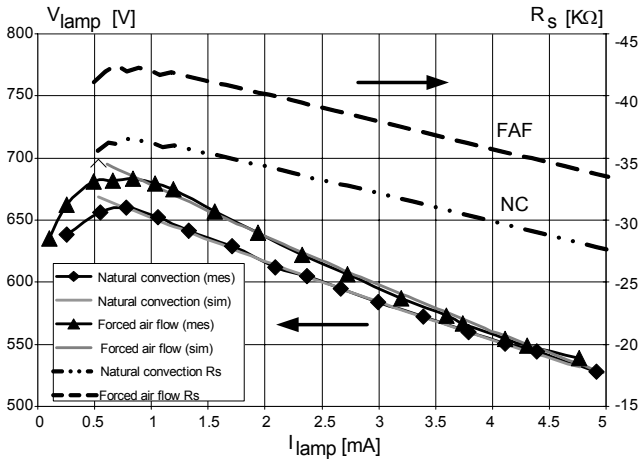


Figure 11. Measured and simulated V-I curves (lower traces) and incremental static resistance,  $R_s$ , upper traces) of experimental CCFL under two thermal operating conditions.  $R_s$  were calculated from fitted V-I curves.

## VII. RESULTS AND DISCUSSION

A very good agreement was found between the measured V-I curves of the lamp and the simulated one by the lamp model of Fig. 9 when applying the extended lamp current source (10) (Fig. 11). These data reveal some interesting features of the CCFL behavior. They show the V-I curve curvature is concave, making the magnitude of the incremental resistance smaller with a current increase. Consequently, one would expect the CCFL-PT system to be more stable at higher lamp current. This implies that the system might be prone to oscillation upon dimming.

The curves of Fig. 11 also show that the magnitude of the negative incremental resistance of the CCFL is decreasing with temperature. This implies that cold lamps will be more prone to instability in a CCFL-PT system. An important observation that can be made this connection, is that V-I under fixed cooling condition represent a range of temperatures, since the lamp temperature will increase with a current increase. Consequently part of the concave change in each V-I curve is due to the temperature change and not just the current change. The relative contribution of each factor (current and temperature) to the curvature has not been assessed in this work.

The good agreement between the experimental and simulated  $ZE_{CCFL}$  verified the validity of the lamp model dynamics. The relatively large scatter of the measured value is probably due to the fact that under the experimental conditions the voltage envelope of the lamp was very small.

The data obtained from the small-signal envelope simulations of the PT and the CCFL were used to generate Nyquist plots of the PT-CCFL LG for two carrier frequencies (49 KHz and 51 KHz) and two temperatures (33°C and 40°C) at a fixed lamp current of 3mA (Figs. 12). The Nyquist plots of Fig. 12a show stable operation of the PT-CCFL system when driven by a carrier that is far from the PT's resonance, however, when  $f_c$  is close to  $f_r$ , the

Nyquist test of Fig. 12b predict unstable operation for 33°C and stable operation for 40°C – as observed experimentally.

The reason for the unstable operation at 33°C is explained by the fact that absolute magnitude of the negative  $R_s(33^\circ\text{C})$  is larger than  $R_s(40^\circ\text{C})$  (local slope of the V-I curves shown in Fig. 11), sufficiently large to satisfy (4).

The thermal effect on the operation of the PT-CCFL system can be explained by considering three possible modes of operation, taking into account the difference between  $f_c$  and  $f_r$ . When  $f_c$  is far from  $f_r$  (Fig. 13a),  $ZE_{CCFL}$  will be smaller than  $ZE_{PT}$ , the lamp will work at its nominal power (P) range and the system is stable. When  $f_c$  is approximately equal to  $f_r$  (Fig. 13b),  $ZE_{PT}$  will have a minima at very low modulating frequency (Fig. 6) where  $ZE_{CCFL}$  is negative, causing the system to be highly unstable. This will cause the lamp current to build up and the system will enter a runaway condition. This operation mode is unsafe from a practical point of view since that the high rms current due to the unrestrained oscillation will cause excessive heat that will eventually damage the CCFL. The third mode of operation will occur at carrier frequencies that are near  $f_r$  causing a moderate instability, that is, LG is slightly more negative than -1 (Fig. 13c). In this mode  $ZE_{CCFL}$  intersects with  $ZE_{PT}$  at a given thermal operating point ( $T_{OP}$ , Fig. 13c). At the intersection point, LG will be exactly -1 and the system will oscillate. The operation of this mode of sustained oscillations will be described by first assuming that  $T < T_{OP}$ , that is,  $ZE_{CCFL} > ZE_{PT}$ . In this case, LG is smaller than -1 and hence the system is unstable which will cause the lamp current to build up. This will heat the lamp and reduce  $ZE_{CCFL}$  (the local slope,  $-R_s$ , around the operating point in Fig. 11) moving the LG toward the (-1, 0) point. When  $LG = -1$  is reached the system will enter the sustained oscillation mode. The lamp rms current in this oscillatory mode ( $I_{rms\_os}$ ) is:

$$I_{rms\_os} = I_{rms\_s} \sqrt{1 + k^2} \quad (12)$$

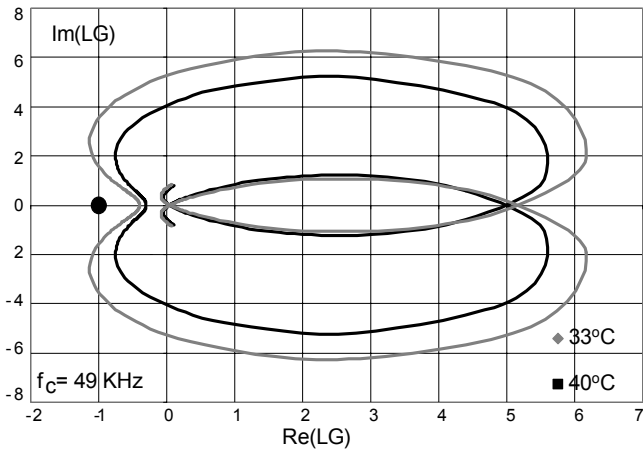
where  $I_{rms\_s}$  is the lamp rms current at stable operation and  $k$  is the envelope AM modulation coefficient.

If the temperature moves to  $T > T_{OP}$ ,  $|LG| < 1$  (Fig. 13c), the system becomes stable and oscillations cease. In this case, the lamp current ( $I_{rms\_s}$ ) is lower than  $I_{rms\_os}$  (12). This will cause the lamp to cool down,  $|ZE_{CCFL}|$  will increase (Fig. 13c) and the operating point will move back to the (-1, 0) point.

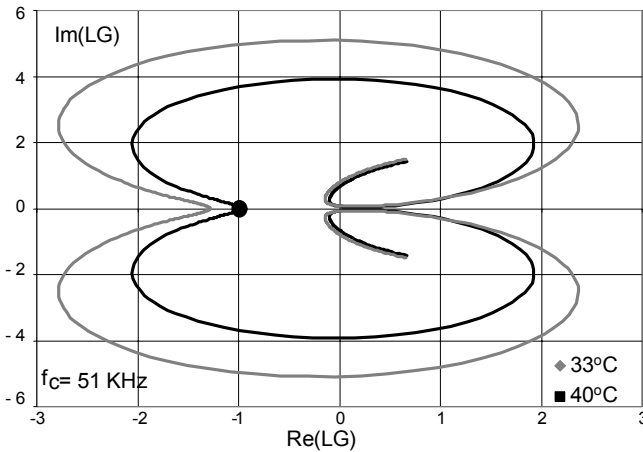
The validity of the models developed in this study was further verified by running a time domain simulation (TRAN) on the CCFL-PT system for the operating condition that should, according to the proposed theory, enter a sustained oscillation condition. The selected operating conditions were:  $f_c = 52.8$  KHz,  $I_{lamp} = 3$  mA,  $T = 40^\circ\text{C}$ . The results of this cycle-by-cycle simulation (Fig. 14) clearly show the sustained oscillations phenomenon, as observed experimentally (Fig. 2).

### VIII. CONCLUSIONS

The envelope analysis concept was applied to investigate the thermal effects in PT-CCFL systems and to delineate their stability criterion. It was found that the main cause for instabilities is the fact that the EI of the PT includes a minimum point at low frequency when  $f_m \approx |f_c - f_r|$ . This minimum is a manifestation of the fact that the PT includes a series resonance branch ( $L_r, C_r$ , Fig. 5) which decreases the output impedance of the PT far sideband frequencies which are close to the resonant frequency of the branch. The negative EI of the CCFL, at low frequencies, was found to decrease with temperature, which makes the system less stable at lower temperatures.

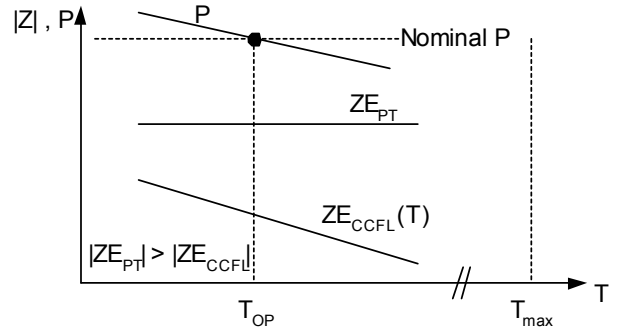


(a)

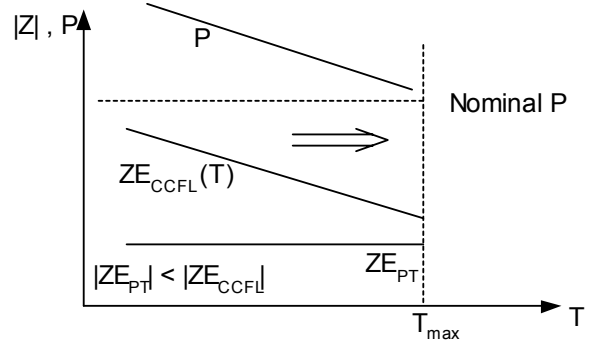


(b)

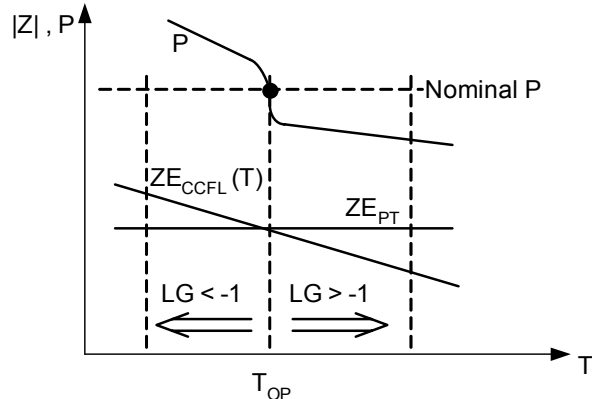
Figure 12. Nyquist plots of experimental PT-CCFL system under different operating conditions (carrier and thermal wise): (a) carrier frequency is far from resonance, stable operation in both thermal operating points, and (b) carrier frequency near resonance, 40°C: stable operation, 33°C: unstable operation.



(a)



(b)



(c)

Figure 13. Possible modes of operation of PT-CCFL system: (a)  $f_c$  far from  $f_r$ , stable mode, (b)  $f_c = f_r$  unstable mode and (c)  $f_c$  near  $f_r$ , oscillations mode.

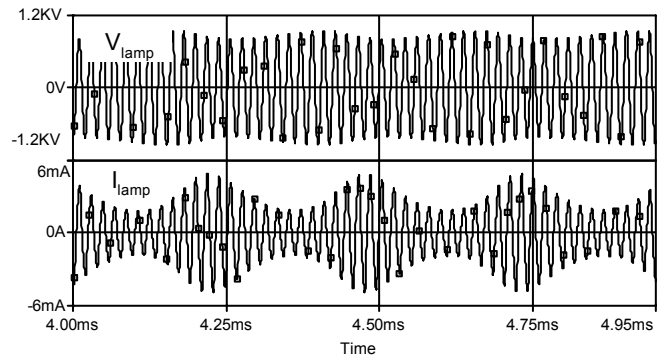


Figure 14. Simulation results, CCFL voltage and current. Same operating conditions as in the experimental of Fig. 2.

This characteristic may cause the system to be unstable at one temperature and stable at a higher temperature. Sustained oscillations are observed when moderate instability are initially present and the oscillations heats up the lamp,  $Z_{E_{CCFL}}$  increases and the system enters the pseudo stable state of  $LG=-1$ .

The findings of this study help to better understand the behavior of PT-CCFL systems and will eventually help to develop methods for stabilizing the system under any desired operating condition.

#### ACKNOWLEDGMENT

This research was supported by THE ISRAEL SCIENCE FOUNDATION (grant No. 113/02) and by the Paul Ivanier Center for Robotics and Production management.

#### REFERENCES

- [1] G. Spiazzi, S. Buso, "Small-signal analysis of cold cathode fluorescent lamp ballasts", *IEEE Power Electronics Specialists Conference, PESC-2005*, 2783-2789, Recife, 2005.
- [2] S. Ben-Yaakov, M. M. Peretz, and S. Lineykin, "Stability of cold cathode fluorescent lamps driven by Piezoelectric Transformers", *IEEE Applied Power Electronics Conference, APEC-2006*, 1517-1522, Dallas, Tx. 2006.
- [3] S. Ben-Yaakov, "Power electronics of piezoelectric elements", professional education seminar presentation, *IEEE Applied Power Electronics Conference, APEC-2006*, Dallas, Tx. 2006.
- [4] C. D. Wey, T. L. Jong and C. T. Pan, "Design and analysis of an SLPT-based CCFL driver", *IEEE Trans. Industrial Electronics*, 50, 1, 208-217, 2003.
- [5] S. Glozman, and S. Ben-Yaakov, "Dynamic interaction analysis of HF ballasts and fluorescent lamps based on envelope simulation". *IEEE Trans. Industry Applications*, 37,5,1531-1536, 2001.
- [6] S. Ben-Yaakov, S. Glozman, and R. Rabinovici, "Envelope simulation by SPICE-compatible models of linear electric circuits driven by modulated signals". *IEEE Trans. Industry Applications*, 37, 2, 527-533, 2001.
- [7] S. Lineykin and S. Ben-Yaakov, "A unified SPICE compatible model for large and small signal envelope simulation of linear circuits excited by modulated signals", *IEEE Power Electronics Specialists Conference, PESC-2003*, 1205-1209, Acapulco, 2003.
- [8] Y. Yin, R. Zane, J. Glaser and R. W. Erickson, "Small-signal analysis of frequency based electronic ballasts", *IEEE Trans Circuits and Systems*, 50, 8, 1103-1110, 2003.
- [9] J. A. Oliver, C. Fernandez, R. Prieto and S. A. Cobos, "Circuit oriented model of rectifiers for large signal envelope simulation", *IEEE Power Electronics Specialists Conference, PESC-2003*, 2771-2776, Recife, 2005.
- [10] S. Ben-Yaakov, M. Shvartsas, and S. Glozman, "Statics and dynamics of fluorescent lamps operating at high frequency: modeling and simulation", *IEEE Trans. Industry Applications*, 38, 6, 1486-1492, 2002.
- [11] M. Gulko, and S. Ben-Yaakov, "Current-sourcing parallel-resonance inverter (CS-PPRI): Theory and application as a discharge lamp driver". *IEEE Trans. Industrial Electronics*, 451, 285-291, 1994.
- [12] Cadence Design Systems, Inc., "Pspice optimizer user's guide", 2<sup>nd</sup> edition, 2000.
- [13] E. Deng and S. C'uk, "Negative incremental impedance and stability of fluorescent lamp", *IEEE Applied Power Electronics Conference, APEC-1997*, 1050-1056, Atlanta, 1997.

- [14] E. Deng, "Negative incremental impedance of fluorescent lamp", Ph. D. dissertation, California Institute of Technology, Pasadena, 1995.



Mor Mordechai Peretz was born in Beer-Sheva, Israel in 1979. He received the B.Tech. degree in Electrical Engineering in 2003 from the Negev Academic College of Engineering, Beer-Sheva, Israel and the M. Sc. degree in Electrical and Computer Engineering from the Ben-Gurion University of the Negev, Israel, in 2005. He is currently a Ph. D. candidate there.

His areas of interests include digital control, switch-mode DC-DC converters, modeling and computer aided design, lighting systems and ballasts, non-linear magnetics and resonant power conversion systems.



Shmuel (Sam) Ben-Yaakov was born in Tel Aviv, Israel in 1939. He received the BSc degree in Electrical Engineering from the Technion, Haifa, Israel, in 1961 and the MS and PhD degrees in Engineering from the University of California Los Angeles, in 1967 and 1970 respectively.

He is presently a Professor at the Department of Electrical and Computer Engineering, Ben-Gurion University of the Negev, Beer-Sheva, Israel, and heads the Power Electronics Group there. He served as the Chairman of that department during the period 1985 - 1989. His current research interests include power electronics, circuits and systems, electronic instrumentation and engineering education. Dr. Ben-Yaakov also serves as Chief Scientist of Green Power Technologies Ltd, Israel, and as a consultant to commercial companies on various subjects, including analog circuit design and Power Electronics.